

XU-YANG WANG<sup>1</sup>, CHENG-WANG TANG<sup>2</sup>, WEN-JIAO DAN<sup>2\*</sup>**EXPERIMENTAL INVESTIGATION OF HYDROGEN EMBRITTLEMENT IN POST-FIRE Q690 WELDMENTS**

The evaluation of the mechanical properties of post-fire high-strength steel welds, particularly for secondary applications in medium- and large-scale infrastructure, is of critical importance in engineering. This study investigates Q690 high-strength steel welds subjected to heat treatment at 300°C, 500°C, 700°C, and 800°C for 20 minutes, followed by air cooling. Electrochemical hydrogen charging, uniaxial tensile testing, and fracture morphology analysis were employed to examine the mechanical properties of these welded components after fire exposure. The effects of hydrogen embrittlement on the mechanical properties and fracture modes of Q690 welds were analyzed, and a hydrogen embrittlement sensitivity index for the welding joints was proposed. The results of the study show that the heat treatment temperature has a significant effect on the hydrogen embrittlement susceptibility of welded structural components. Higher heat treatment temperatures and longer hydrogen charging times lead to a decrease in the mechanical properties of the material, which is characterised by a flatter and smoother macroscopic fracture surface, while the microscopic fracture pattern is characterised by micro-voids. Hydrogen-induced deformation leads to the accumulation of structural defects, such as micro-inhomogeneities and micro-voids, due to increased hydrogen concentrations. Consequently, the material's resistance to brittle failure is diminished.

*Keywords:* Q690 weldment; Heat treatment; mechanical properties; hydrogen embrittlement sensitivity; fracture morphology

**1. Introduction**

High-strength steels are essential for constructing high-rise buildings and long-span structures due to their excellent strength, ductility, lightweight properties, and remarkable earthquake resistance [1]. However, the increasing size and complexity of buildings, coupled with greater fire intensity, negatively affect the mechanical properties of these steels [2-4]. Zhao et al. [5] demonstrated that induction tempering of Q690 steel accelerates heating rates, reduces energy consumption, and enhances the microstructure and mechanical properties more effectively than conventional methods. Li et al. [6] studied the influence of post-weld heat treatment (PWHT) on carbide precipitation and impact characteristics in the coarse-grained heat-affected zone (CGHAZ) of Q690. They observed tempering embrittlement at PWHT temperatures of 520-570°C, which increased crack initiation rates during rapid loading. Dan et al. [7] investigated the cooling effects (300-800°C) on Q345, Q460, Q550, and Q690 steels, proposing a predictive equation and noting a significant reduction in mechanical properties above 600°C. Tang et al. [8] developed a stress-strain relationship model for structural

steel exposed to fire, highlighting decreased mechanical properties after cooling from temperatures above 500°C, although fire-affected bridges often retain sufficient strength. Chiew et al. [9] explored secondary heating effects on S690 steel plates and found considerable strength loss at higher temperatures, whereas performance below 400°C remained stable. Villalobos et al. [10] examined hydrogen tempering in alloy steel, reporting strengths of 700-900 MPa and ductility of 9-11% in untempered steel, while tempered steel displayed reduced strengths of 650-850 MPa.

Hydrogen embrittlement (HE) presents significant challenges for high-strength steels in hydrogen-rich environments, often causing brittle fractures under stress levels well below the yield strength. Post-fire conditions can promote hydrogen gas production via complex chemical reactions. Liu et al. [11] employed slow strain rate tensile tests to demonstrate how hydrogen diffusion and accumulation increase material brittleness. Wang et al. [12] studied notch tensile strength in bearing steel (yield strength: 1305 MPa) under electrochemical hydrogen charging and found strength reductions correlated with increased hydrogen concentrations, particularly under high stress concen-

<sup>1</sup> SHANGHAI JIAO TONG UNIVERSITY, SCHOOL OF OCEAN AND CIVIL ENGINEERING, SHANGHAI, 200240, P.R. CHINA

<sup>2</sup> ANHUI SCIENCE AND TECHNOLOGY UNIVERSITY, SCHOOL OF MECHANICAL ENGINEERING, CHUZHOU, 233100, P.R. CHINA

\* Corresponding author: danwj017@163.com



tration factors. Tiwari et al. [13] introduced a novel hydrogen charging method using a hydrogen-saturated segment as a cathode in an alkaline solution under uniaxial loading. This method showed that hydrogen alters mechanical properties by occupying traps such as dislocations and grain boundaries. Djukic et al. [14] explored HE mechanisms in structural carbon steel, identifying hydrogen-induced dissociation (HEDE) and hydrogen-enhanced local plasticity (HELP) as processes dependent on local hydrogen concentrations. Wang et al. [15] analyzed the relationships among threshold stress intensity, crack propagation rates, and the hydrogen diffusion coefficient in 30CrMnSiNi2 steel. Their results indicated that yield strengths above 1360 MPa are unaffected by the diffusion coefficient, while below this threshold, higher diffusion coefficients increased threshold stress intensity and decreased crack propagation rates. Allen et al. [16] conducted tensile tests on two types of advanced high-strength steel (AHSS) after hydrogen charging, using molecular microscopy to measure hydrogen concentrations. Their model linked hydrogen diffusion and mechanical property degradation, introducing a two-factor approach to predict recovery from embrittlement. Venezuela et al. [17] found that hydrogen reduced ductility and promoted shear fractures in MS1700 martensitic high-strength steel, attributing its susceptibility to hydrogen embrittlement to its high carbon content and martensitic structure, which facilitate hydrogen trapping. Saha et al. [18] studied hydrogen embrittlement in medium-carbon high-strength steel at varying tempering temperatures, revealing that dislocation density and precipitate morphology strongly influence HE sensitivity.

This study investigates the sensitivity of heat-treated Q690 high-strength steel weldments to hydrogen embrittlement through electrochemical hydrogen charging and uniaxial tensile testing, complemented by scanning electron microscopy (SEM) for fracture morphology analysis. The research explores the influence of hydrogen charging duration on embrittlement properties, examining hydrogen diffusion, hydrogen-induced damage, and the mechanisms behind transformation and fracture modes. An improved hydrogen embrittlement testing method was developed to accurately assess the embrittlement resistance of Q690 weldments. This approach provides insights into hydrogen diffusion and accumulation in Q690 steel and their effects on mechanical properties, helping to mitigate structural failures and extend the service life of Q690 steel in applications such as bridges, buildings, ships, and other critical infrastructure.

## 2. Materials and Experiments

The material selected for this study was Q690 high-strength steel weldments. The sample consisted of sheet metal with a total length of 100 mm and a thickness of 4 mm. The chemical composition of the material is provided in TABLE 1, while the sample dimensions are illustrated in Fig. 1 [19]. A 25 mm hydrogen charging section was positioned at the center of the sample. Prior to welding, a 60° V-groove with a depth of 2.5 mm was milled along the joint interface. The groove dimensions are depicted in Fig. 2.

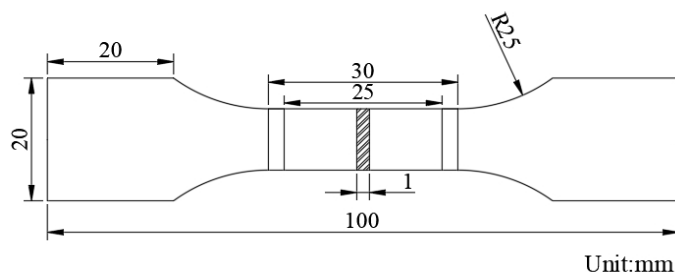


Fig. 1. Schematic diagram of weldment specimen and beveling

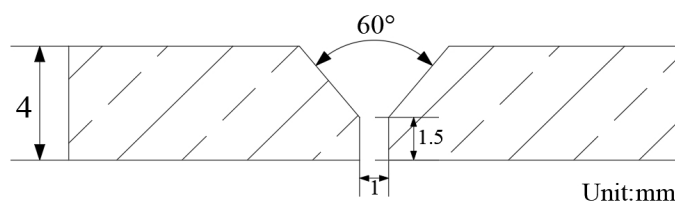


Fig. 2. Welding Bevel Schematic

Welding was conducted using carbon dioxide gas-shielded welding (80% Ar + 20% CO<sub>2</sub>) with a welding current of 200 A and a voltage of 22 V. The material was allowed to cool naturally to room temperature after welding. The welding wire used in this experiment was MG80-G, which conforms to the GB/T-39281 [20] standard. This solid welding wire, protected by mixed gas, is specifically designed for high-strength steel and has a diameter of 1.2 mm. The chemical composition of the welding wire is presented in TABLE 2 [21].

The heat treatment experiments were conducted with four groups, each comprising five standard samples, resulting in a total of 20 samples. For the tensile tests, three samples were tested at each temperature and hydrogen charging duration, while

TABLE 1

Q690 high strength steel chemical composition table (mass fraction %)

Chem. Comp.	C	Si	Mn	S	P	Nb	V	Ti	Cr	Ni	Mo	B
vValue	≤0.18	≤0.6	≤2.0	≤0.03	≤0.03	≤0.11	≤0.12	≤0.2	≤1.0	≤0.8	≤0.3	≤0.004

TABLE 2

Chemical composition table of welding wire (mass fraction %)

Chem. Comp.	C	Mn	Si	S	P	Cr	Ni	Mo	Cu
Value	≤0.11	1.40~1.85	0.40~1.00	≤0.025	≤0.025	0.25~0.60	1.20~2.40	0.20~0.60	≤0.50

two additional samples were used for fracture analysis. The Q690 high-strength steel welded parts were heated in a muffle furnace at a rate of 20°C/min to target temperatures of 300°C, 500°C, 700°C, and 800°C. Each sample was maintained at the designated temperature for 20 minutes before being removed and air-cooled to room temperature. The experimental data and corresponding specimens are shown in Fig. 3.

The Q690 welded parts were polished using SiC sandpaper, progressing sequentially from grit 200 to grit 2000. The polished samples were then rinsed with alcohol and dried with cold air. The remaining sections of the test pieces were coated with epoxy resin to prepare a defined hydrogen charging surface. The hydrogen charging section measured 25 mm in length and 10 mm in width, resulting in a total charging area of 2.5 cm<sup>2</sup>, as illustrated in Fig. 4(a).

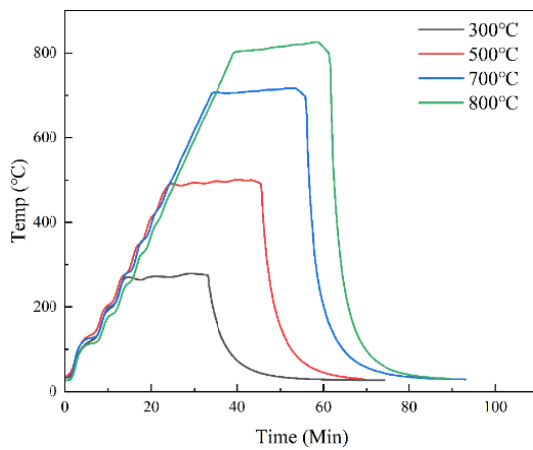
The electrolyte was prepared by dissolving 1 g/L CH<sub>4</sub>N<sub>2</sub>S in a 0.5 mol/L H<sub>2</sub>SO<sub>4</sub> solution, forming a mixed solution of the

two compounds. During the hydrogen charging experiments, the sample was connected to the cathode, and a platinum plate was used as the anode. The electrolyte temperature was maintained between 20°C and 25°C. The detailed hydrogen charging plan is provided in TABLE 3, while the schematic diagram of the hydrogen charging apparatus is shown in Fig. 4(b).

TABLE 3

Electrochemical hydrogen charging experimental program

Heat treatment temperature (°C)	Hydrogen charging time (h)
300	0.167, 0.5, 1, 2
500	
700	
800	



(a)

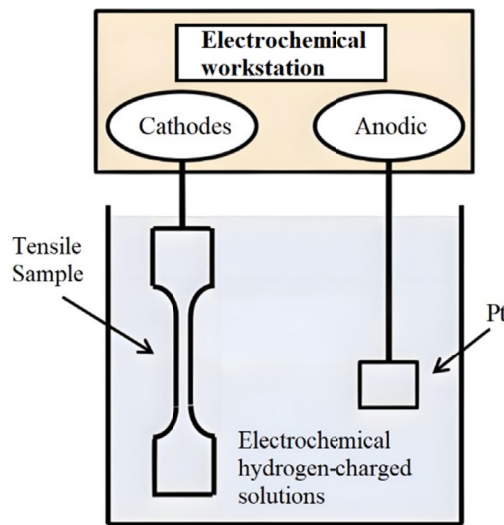


(b)

Fig. 3. Specimen heat treatment (a) Heat treatment process data and (b) Specimens after the heat treatment



(a)



(b)

Fig 4. Q690 high strength steel weldment specimen drawing (a) Specimens for Electrochemical hydrogen charging and (b) Schematic diagram of Electrochemical hydrogen charging

Electrochemical hydrogen charging experiments were conducted for equal durations at each heat treatment temperature to evaluate the hydrogen-induced damage in Q690 high-strength steel welded parts. The mechanical properties of the samples were analyzed alongside the impact of hydrogen molecules on the material's mechanical integrity following hydrogen charging. The tests were carried out at 300°C, 500°C, 700°C and 800°C with electrochemical hydrogen charging times of 0.167 h, 0.5 h, 1 h and 2 h, respectively [22]. The specific electrochemical hydrogen charging experimental protocols are shown in TABLE 3.

In uniaxial tensile testing, the sample was subjected to tensile evaluation at room temperature immediately after the completion of the electrochemical hydrogen charging test. To minimize hydrogen loss from the sample, the entire uniaxial tensile test was completed within twenty minutes. The tensile tests were performed using a SuSiUT5105 electronic universal testing machine, which has a maximum tensile force capacity of 100 kN and operates at a tensile rate of 3 mm/min. These tests were conducted in strict accordance with GB/T 228-1987, Tensile Test Methods for Metals [23].

Fracture morphology refers to the distinctive surface characteristics formed when a material undergoes failure, providing a detailed reflection of its mechanical behavior, microstructure, and fracture mechanisms at the moment of failure. By closely examining and analyzing the microstructural features of the fracture surfaces in Q690 high-strength steel welded parts, valuable insights into the causes and progression of material failure can be obtained.

For this study, fractured Q690 high-strength steel welded parts were analyzed using a Zeiss EVO18 scanning electron microscope (SEM) to conduct a detailed examination of the fracture surface. This analysis specifically focused on the fractographic characteristics and transformation patterns within the overall fracture morphology of the Q690 high-strength steel welded parts subjected to electrochemical hydrogen charging under various heat treatment conditions.

### 3. Experimental results and discussion

During the heat treatment of high-strength steel, an increase in temperature within a specific range typically results in a gradual increase in grain size, which generally leads to a reduction in the steel's strength [24]. Fig. 5(a) presents the tensile stress-strain curves for Q690 high-strength steel weldments subjected to various heat treatment temperatures. The data show that the Q690 weldments without heat treatment at room temperature exhibit the highest tensile strength, yield strength, and elongation at break. However, as the heat treatment temperature increases, a noticeable decline in the material's mechanical properties is observed [25,26]. At elevated temperatures, fractures typically occur in the weld zone, which may be attributed to welding defects, such as porosity. When the post-fire joint is subjected to hydrogen exposure, the fracture location shifts to the heat-affected zone. This suggests that the weld joint becomes significantly more brittle at higher temperatures, which reduces the overall elongation of the welded material [27].

Fig. 5(b) shows the linear trends for the ultimate tensile strength ( $\sigma_b$ ), yield strength ( $\sigma_s$ ), and elongation at break ( $\delta$ ) of the material. It is important to note that when the heat treatment temperature reaches 800°C, the mechanical properties of Q690 welds drop to their lowest values. Specifically,  $\sigma_b$  decreases from the initial 763.09 MPa to 524.68 MPa,  $\sigma_s$  from 695.98 MPa to 463.71 MPa, and  $\delta$  from 26.88% to 18.52%. The reduction in tensile strength and yield strength of Q690 welds follows a consistent trend, although the decline is relatively gradual. It has been observed that, after high-temperature heat treatment, precipitates in the carbon-rich zones of welded joints become coarser and more numerous [28]. In welded joints, precipitation in carbon-rich zones leads to an increase in carbon content within the weld zone, which subsequently results in reduced material elongation. This effect is attributed to the carbon solution strengthening mechanism [29].

The comprehensive tensile data of the specimen are shown in TABLE 3. The loss rate of tensile strength ( $\Delta\sigma_b$ ), yield strength

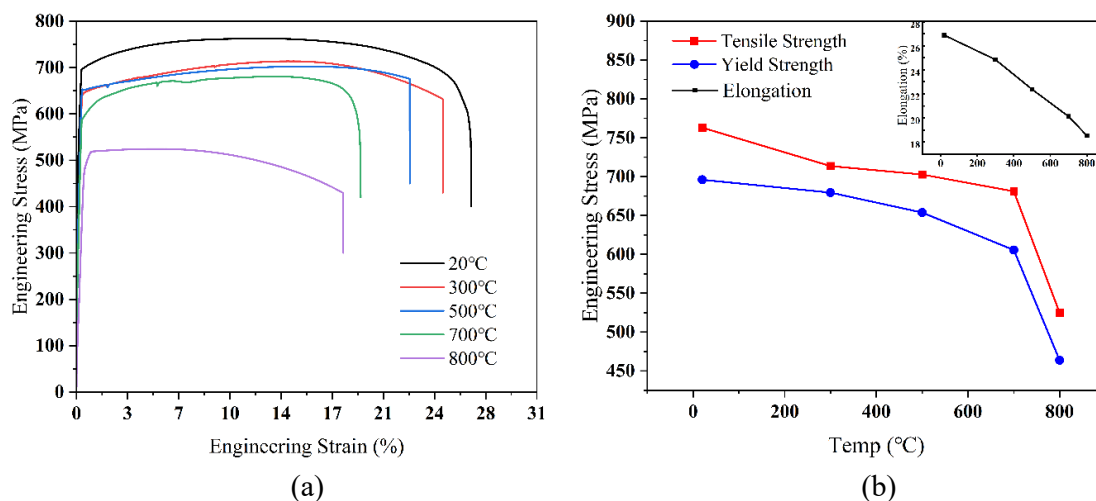


Fig. 5. Mechanical properties of Q690 weldments after various heat treatment temperatures (a) Stress-strain curves and (b) Mechanical parameters vs heat treatment temperature

( $\Delta\sigma_s$ ) and elongation at break ( $\Delta\delta$ ) at different heat treatment temperatures is calculated as follows:

$$\Delta\sigma_b = |(\sigma_b - \sigma_{b0})/\sigma_{b0}| \quad (1)$$

$$\Delta\sigma_s = |(\sigma_s - \sigma_{s0})/\sigma_{s0}| \quad (2)$$

$$\Delta\delta = |(\delta - \delta_0)/\delta_0| \quad (3)$$

In these formulas,  $\sigma_b$ ,  $\sigma_s$  and  $\delta$  denote the parameters after hydrogen charging, while  $\sigma_{b0}$ ,  $\sigma_{s0}$  and  $\delta_0$  represent the parameters prior to hydrogen charging. According to the calculations, the tensile strength of the material decreased by approximately 31%, the yield strength by about 33%, and the elongation at break by roughly 31%.

Hydrogen damage is one of the most complex phenomena that significantly contribute to the degradation of the mechanical properties of metallic materials. Unlike degradation processes that occur in the absence of hydrogen, the kinetics of hydrogen damage introduce a wide range of new and often unknown factors, which complicate the understanding of the material's behavior under stress [30]. In order to investigate the hydrogen damage performance of Q690 weldments subjected to different heat treatment temperatures, electrochemical hydrogen charging

experiments were performed on these post-fire welded components. The experiments were conducted under identical time conditions to thoroughly assess the effect of hydrogen molecules on the damage mechanisms affecting the Q690 welded parts.

Fig. 6 presents the tensile test curves for Q690 high-strength steel weldments subjected to electrochemical hydrogen charging after various heat treatment temperatures. At 300°C, as hydrogen charging time increases, tensile strength gradually decreases (Fig. 6a). At 500°C, tensile strength and elongation 0.167 hours of hydrogen charging are similar to those of uncharged material. However, the elongation at break decreased significantly at the time of hydrogen charging for 2 h (Fig. 6b). These results for both uncharged and hydrogen-charged samples clearly show that electrochemical hydrogen charging significantly reduces both tensile strength and elongation, increasing susceptibility to hydrogen embrittlement [31]. As shown in Fig. 6(c), the tensile strength of welded parts without hydrogen charging at 700°C and those subjected to 0.167 hours of hydrogen charging are nearly identical. However, when the charging time is extended to 2 hours, both tensile strength and elongation decrease significantly. During electrochemical hydrogen charging, hydrogen atoms diffuse and accumulate at stress concentrators and localized defects, reduc-

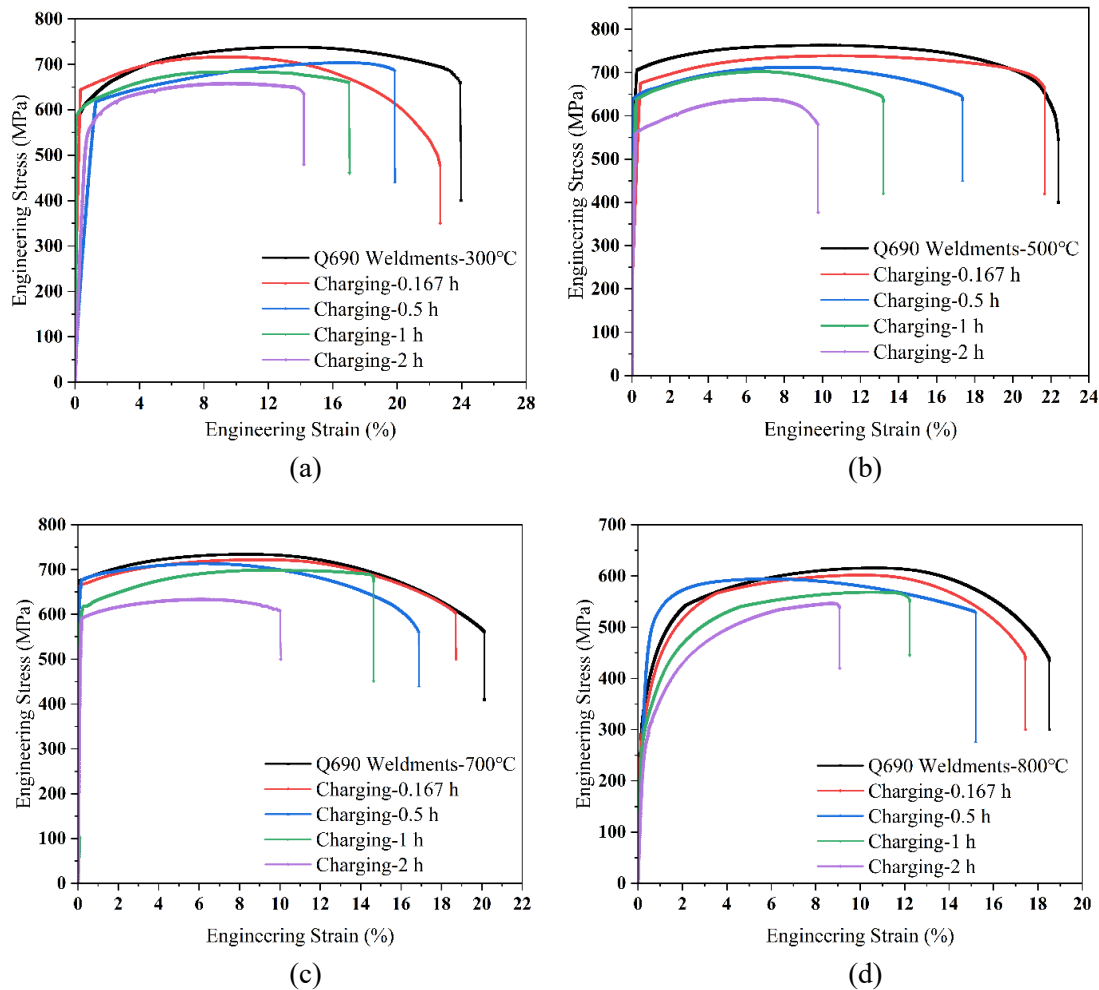


Fig. 6. Tensile diagram of mechanical properties of Q690 weldments with different hydrogen charging times. (a) 300°C, (b) 500°C, (c) 700°C and (d) 800°C

ing toughness [32]. Hydrogen molecules enhance plastic sliding through the Hydrogen Enhanced Localized Plasticity (HELP) mechanism, promoting hydrogen-induced cracks and localized embrittlement [33,34]. Even with localized plastic deformation, hydrogen can lead to brittle fracture, further reducing the material's strength and elongation [35].

Fig. 7 shows the variation in tensile strength (Fig. 7a), yield strength (Fig. 7b), and elongation at break (Fig. 7c) as a function of hydrogen charging time at different heat treatment temperatures. As seen in Fig. 7a, the tensile strength decreases consistently with increasing hydrogen charging time at all heat treatment temperatures. At 800°C, a significant strength reduction of about 8% is observed due to hydrogen exposure. Figs. 7b and 7c further illustrate the changes in yield strength and ductility. After heating to 800°C and charging with hydrogen for 2 hours, the yield strength of the Q690 high-strength steel welded parts is 525.17 MPa, and the ductility is 9.08%. Compared to the uncharged condition, yield strength decreases by approximately 11%, while elongation drops by about 51%. This substantial reduction in ductility may be attributed to the higher pearlite content and smaller grain size of the material, which alter its tensile behavior [36]. Molecular hydrogen significantly compromises both ductility and strength, promoting hydrogen-

induced cracking and potentially leading to catastrophic brittle failure, even below the material's yield stress [37].

TABLES 4-7 present the calculated residual coefficients for tensile strength, yield strength, and elongation at break of materials subjected to various hydrogen charging times, following heat treatment at 300°C, 500°C, 700°C, and 800°C. The impact of hydrogen exposure is primarily seen as a reduction in toughness and the onset of brittle fracture. As hydrogen charging time and heat treatment temperature increase, the residual values for tensile strength, yield strength, and elongation of the Q690 welded parts show distinct trends. Notably, heat treatment temperature strongly influences the elongation at break. As shown in TABLE 4, when the heat treatment temperature is 300°C, the elongation at break after electrochemical hydrogen charging decreases from an initial 24.85% to 14.2%, corresponding to a ductility loss of approximately 43%. At 800°C, post-fracture elongation is further reduced from 18.52% to 9.08%, resulting in a ductility loss of about 51% (TABLE 7). With increasing heat treatment temperature, the material's hydrogen embrittlement (HE) sensitivity rises, particularly with longer hydrogen charging times. Previous studies have shown that hydrogen accumulates preferentially at the central austenite grain boundaries, significantly weakening their cohesion strength [38].

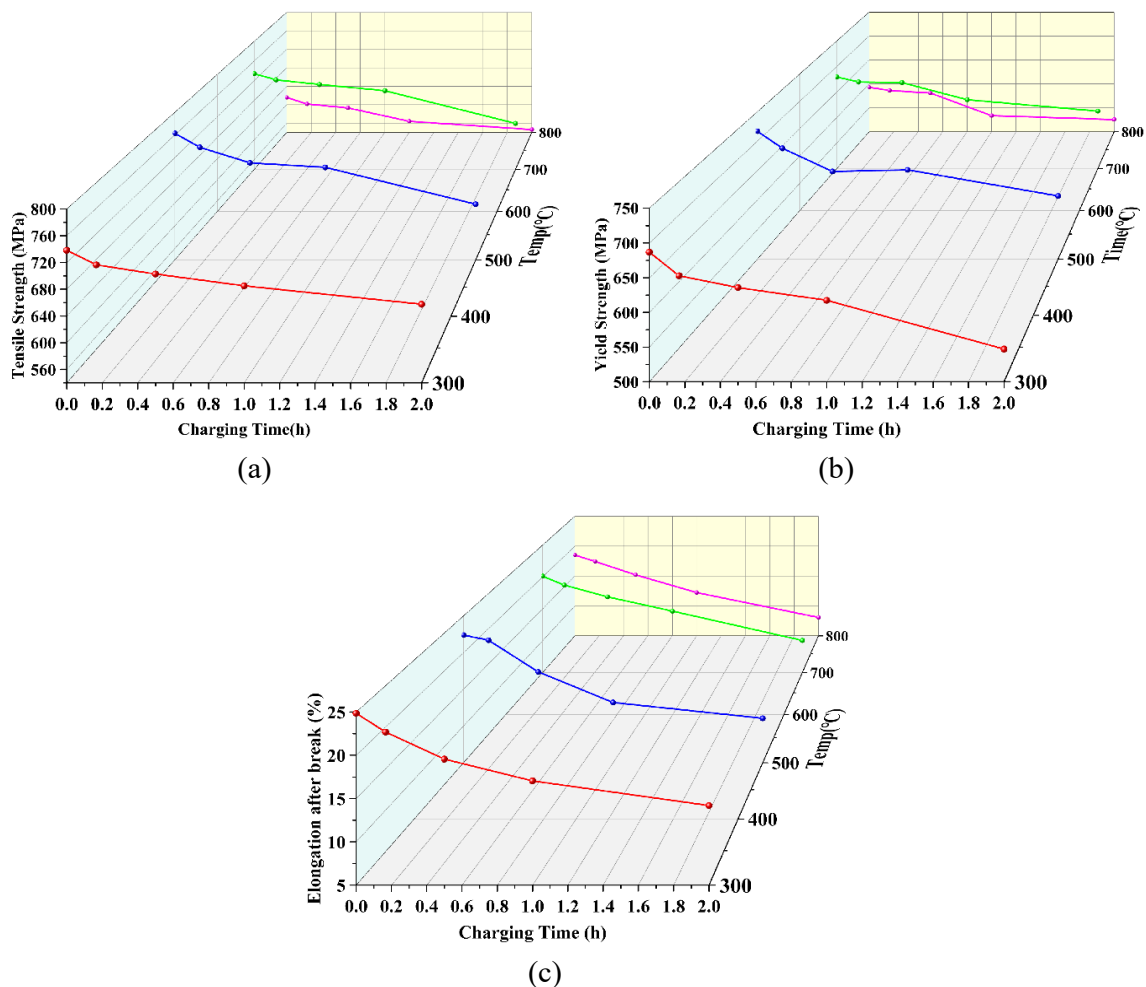


Fig. 7. Mechanical behaviors degradation of post-fire Q690 weldments with hydrogen charging time. (a) Tensile strength, (b) yield strength, and (c) elongation

TABLE 4

Mechanical properties residual factors of post-fire Q690 weldments after different hydrogen charging (300°C)

Temp	$\sigma_b$ (MPa)	$\sigma_s$ (MPa)	$\delta$ (%)	$\sigma_b/\sigma_{b0}$	$\sigma_s/\sigma_{s0}$	$\delta/\delta_0$
300°C	738.23	686.79	24.85	1	1	1
300°C-Charging -0.167 h	716.37	652.86	22.68	0.97	0.95	0.91
300°C-Charging -0.5 h	702.76	635.74	19.86	0.95	0.93	0.80
300°C-Charging -1 h	685.06	617.47	17.04	0.93	0.90	0.69
300°C-Charging -2 h	657.58	547.11	14.20	0.89	0.80	0.57

TABLE 5

Mechanical properties residual factors of post-fire Q690 weldments after different hydrogen charging (500°C)

Temp	$\sigma_b$ (MPa)	$\sigma_s$ (MPa)	$\delta$ (%)	$\sigma_b/\sigma_{b0}$	$\sigma_s/\sigma_{s0}$	$\delta/\delta_0$
500°C	763.09	716.94	22.38	1	1	1
500°C-Charging -0.167 h	738.43	687.95	21.68	0.97	0.96	0.97
500°C-Charging -0.5 h	711.07	668.47	17.36	0.93	0.93	0.78
500°C-Charging -1 h	703.15	651.27	13.20	0.92	0.91	0.60
500°C-Charging -2 h	638.20	606.89	9.77	0.84	0.85	0.44

TABLE 6

Mechanical properties residual factors of post-fire Q690 weldments after different hydrogen charging (700°C)

Temp	$\sigma_b$ (MPa)	$\sigma_s$ (MPa)	$\delta$ (%)	$\sigma_b/\sigma_{b0}$	$\sigma_s/\sigma_{s0}$	$\delta/\delta_0$
700°C	734.37	679.54	20.12	1	1	1
700°C-Charging -0.167 h	721.83	669.61	18.72	0.98	0.99	0.93
700°C-Charging -0.5 h	712.36	668.34	16.88	0.97	0.98	0.84
700°C-Charging -1 h	699.70	644.79	14.64	0.95	0.95	0.73
700°C-Charging -2 h	633.33	612.56	10.04	0.86	0.90	0.48

TABLE 7

Mechanical properties residual factors of post-fire Q690 weldments after different hydrogen charging (800°C)

Temp	$\sigma_b$ (MPa)	$\sigma_s$ (MPa)	$\delta$ (%)	$\sigma_b/\sigma_{b0}$	$\sigma_s/\sigma_{s0}$	$\delta/\delta_0$
800°C	615.88	593.12	18.52	1	1	1
800°C-Charging -0.167 h	601.66	586.16	17.44	0.98	0.99	0.94
800°C-Charging -0.5 h	593.26	580.98	15.20	0.96	0.98	0.82
800°C-Charging -1 h	569.28	553.74	12.24	0.92	0.93	0.66
800°C-Charging -2 h	546.39	525.17	9.08	0.89	0.89	0.49

Hydrogen molecules influence the elongation of the specimens, with various parameters sensitive to hydrogen embrittlement serving as indicators of hydrogen's effects on steel. The sensitivity to hydrogen embrittlement is quantified by the index  $I_{HE}(\delta)$  [39], defined as:

$$I_{HE}(\delta) = 1 - \delta_H/\delta_0 \times 100\% \quad (4)$$

$\delta_0$  represents the elongation without hydrogen charging, and  $\delta_H$  denotes the elongation following hydrogen exposure. The rate of decrease in hydrogen-induced elongation of the material is encapsulated by  $I_{HE}(\delta)$ . A higher value of  $I_{HE}(\delta)$  indicates poorer resistance to hydrogen embrittlement and greater sensitivity to its effects. Fig. 8 shows the trend of the hydrogen embrittlement sensitivity index for Q690 high-strength steel weldments as the heat treatment temperature increases, under constant hydrogen charging time conditions. The data reveal that for any given hydrogen charging duration, the hydrogen embrittlement sensitivity coefficient of Q690 welded components increases consistently with temperature. Specifically, at a hydrogen charging time of 0.167 hours, the material's plasticity decreases, and its sensitivity to hydrogen embrittlement rises from 15.63% at 300°C to 35.12% at 800°C. When the hydrogen charging time is extended to 2 hours, the hydrogen embrittlement sensitivity index increases significantly, from 47.17% at 300°C to 66.22% at 800°C. According to the NASA 8-30744 [40] standard for assessing alloy hydrogen damage in the United States, the hydrogen embrittlement sensitivity index ( $I_{HE}(\delta)$ ) of the experimental steel exceeds 50% when the hydrogen charging time reaches 1 hour. This indicates severe hydrogen damage in the samples subjected to an electrochemical hydrogen charging duration of 1 hour. The diffusion depth of hydrogen can be calculated using the formula:

$$d = \sqrt{2Dt} \quad (5)$$

where  $D$  represents the hydrogen diffusion coefficient in the material and  $t$  is the corresponding electrochemical hydrogen charging time. Notably, the diffusion coefficient of hydrogen in alpha iron at room temperature is relatively high, approximately  $10^{-4} \text{ cm}^2 \cdot \text{s}^{-1}$  [41]. Based on calculations, the hydrogen diffusion depths for Q690 high-strength steel welded components after hydrogen charging for 0.167 hours, 0.5 hours, 1 hour, and 2 hours are 0.0334 mm, 0.1 mm, 0.2 mm, and 0.4 mm, respectively. Several factors contribute to the reduction in plasticity of steel due to hydrogen damage following electrochemical hydrogen charging tests. First, the diffusion of hydrogen molecules into the metal weakens the material's structure by reducing the binding forces between metal atoms. Second, aggregated hydrogen molecules may combine to form hydrogen gas or hydrides within the metal, introducing additional stress due to volume changes. Lastly, the presence of hydrogen molecules reduces the surface bonding strength of the metal, promoting crack formation and propagation, further compromising the material's integrity.

Fig. 9 shows scanning electron microscopy (SEM) images of the fracture surfaces of Q690 welded tensile samples subjected to different hydrogen charging times and heat treatment condi-

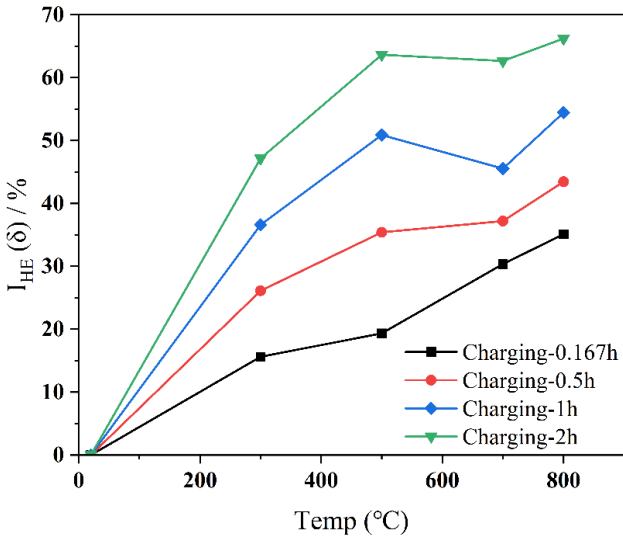


Fig. 8. Hydrogen embrittlement susceptibility index of post-fire Q690 steel

tions. Notably, the tensile fractures consistently occur within the heat-affected zone. As seen in the figure, the macroscopic fracture surface of the sample without hydrogen charging at room temperature is rough, while the microscopic fracture features multiple dimples (Fig. 9a), indicative of a typical ductile fracture with uniform size. At a heat treatment temperature of 300°C and 2 hours of hydrogen charging, the macroscopic fracture surface becomes smoother, with necking suggesting plastic deformation. Microscopic analysis reveals increased toughness pits, indicating that the sample has not yet reached complete brittle fracture. At higher temperatures (700°C) with 2 hours of hydrogen charging, the macroscopic fracture surface is flat and smooth, displaying corrugations and localized cracks. The microscopic fracture surface appears smoother after hydrogen charging. As the heat treatment temperature increases, the microscopic surface becomes rougher, adopting a relief-like structure. The hydrogen-charged samples fail through a deconstructive fracture mechanism, with widespread tearing and distinct brit-

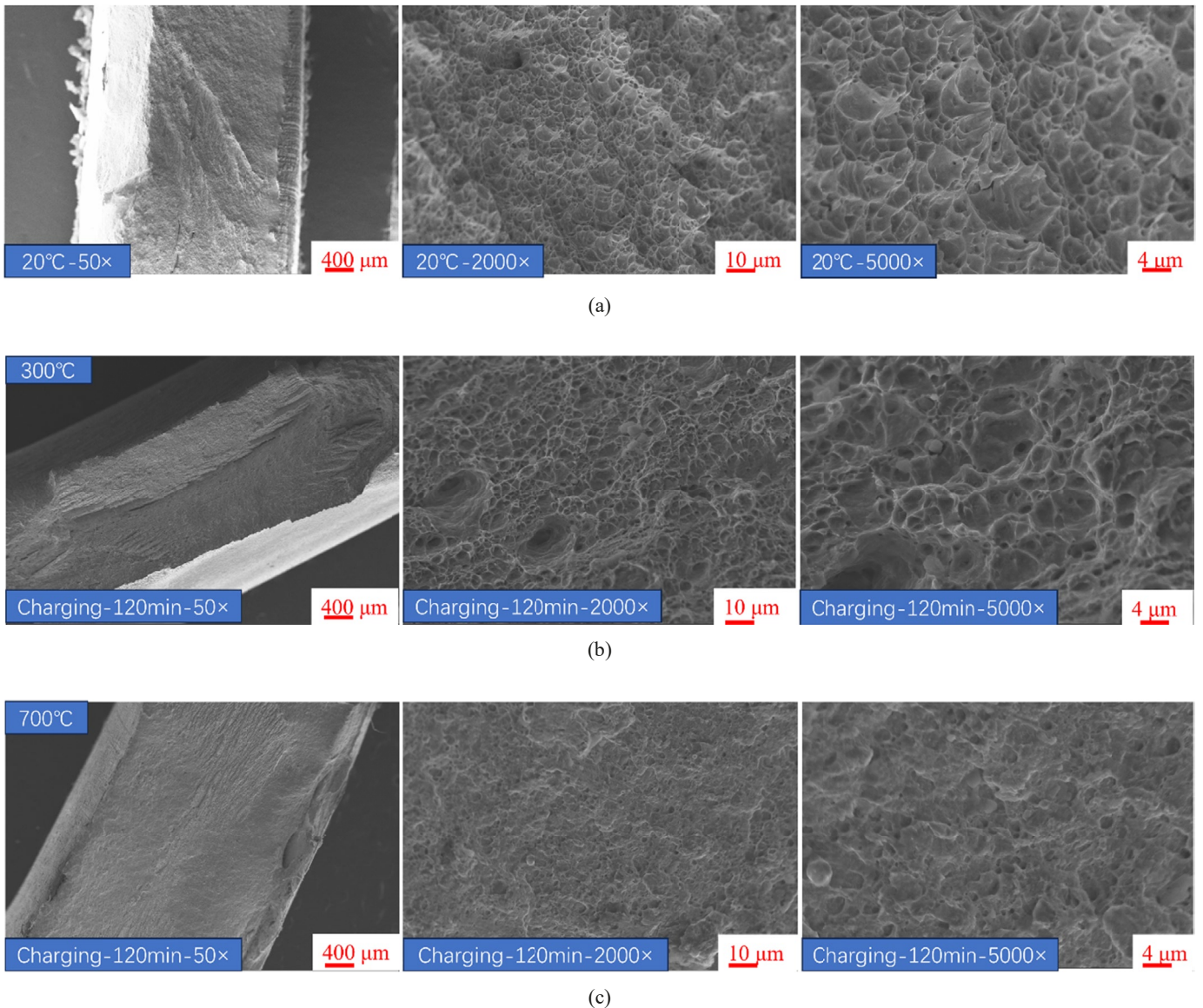


Fig. 9. Fracture morphology of hydrogen charging weldment with different heat treatment temperatures for 2h (×50, ×2000 and ×5000) (a) at 20°C, (b) at 300°C, (c) at 700°C

tle fracture characteristics. These observations demonstrate that as the heat treatment temperature and hydrogen charging time increase, the extent of hydrogen damage intensifies, resulting in a gradual transition from ductile to brittle fracture.

#### 4. Conclusions

This study investigates the hydrogen embrittlement sensitivity of post-fire Q690 high-strength steel welds using electrochemical hydrogen charging, uniaxial tensile testing, and scanning electron microscopy (SEM) to analyze fracture morphology. The key findings are as follows:

- (1) As the heat treatment temperature increases, the mechanical properties of post-fire Q690 high-strength steel welds significantly deteriorate. Key properties such as tensile strength, yield strength, and elongation at break decline rapidly at higher temperatures, leading to deformation, fracture, and other forms of damage. Between 300°C and 500°C, the effects on tensile and yield strength are minimal. However, when the temperature reaches 700°C to 800°C, a marked deterioration in both strength and elongation is observed.
- (2) As the hydrogen concentration in the solution increases with longer electrochemical hydrogen charging, hydrogen atoms infiltrate the internal structure of the welds, further degrading the material's mechanical properties. Notably, when the hydrogen charging time exceeds 1 hour, there is a significant reduction in elongation at fracture, and the hydrogen embrittlement sensitivity coefficient increases, leading to more pronounced hydrogen-induced damage.
- (3) After electrochemical hydrogen charging, a significant amount of hydrogen molecules is adsorbed on the surface and diffuses into the material's interior, accumulating within the structure. As a result, the macroscopic fracture surface becomes smoother, while the microscopic fracture exhibits ductile characteristics, primarily micro-pores. The influence of hydrogen on material deformation leads to the accumulation of structural defects, including fracture inhomogeneity and micro-pore formation. This increased hydrogen concentration ultimately reduces the material's resistance to brittle failure.

#### REFERENCES

- [1] C. Zhang, R. Wang, G. Song. Effects of pre-fatigue damage on mechanical properties of Q690 high-strength steel. *Constr. Build. Mater.* **252**, 118845 (2020). DOI: <https://doi.org/10.1016/j.conbuildmat.2020.118845>
- [2] Arthur C. Reardon, ed. *Metallurgy for the Non-metallurgist*. Asm International (2011).
- [3] J. Chen, B. Young, B. Uy, Behavior of high strength structural steel at elevated temperatures. *J. Struct. Eng.-ASCE*, **132** (12), 1948-1954 (2006). DOI: [https://doi.org/10.1061/\(asce\)0733-9445\(2006\)132:12\(1948\)](https://doi.org/10.1061/(asce)0733-9445(2006)132:12(1948))
- [4] X. Qiang, F.S.K. Bijlaard, H. Kolstein, Deterioration of mechanical properties of high strength structural steel S460N under transient state fire condition. *Mater. Design* **40**, 521-527(2012). DOI: <https://doi.org/10.1016/j.matdes.2011.11.069>
- [5] L.P. Zhao, H.M. Zhang, W. Liu, et al. Effect of different tempering processes on microstructure and hardness of Q690 steel. *Adv. Mater. Res.* **721**, 49-53 (2013). DOI: <https://doi.org/10.4028/www.scientific.net/AMR.721.49>
- [6] Z.S. Li, S.L. Li, L. Tian, et al., Effect of post-weld heat treatment on carbide precipitation and impact properties of coarse-grained heat-affected zone of Q690 steel. *Adv. Mater. Res.* **989**, 576-580 (2014). DOI: <https://doi.org/10.4028/www.scientific.net/amr.989-994.576>
- [7] W.J. Dan, R.B. Gou, M. Yu, et al., Experimental study on the post-fire mechanical behaviours of structural steels. *J. Constr. Steel Res.* **199**, 107629 (2022). DOI: <https://doi.org/10.1016/j.jcsr.2022.107629>
- [8] Z. Tang, T. Wei, Y. Ma, et al., Residual strength of steel structures after fire events considering material damages. *Arab. J. Sci. Eng.* **44**, 5075-5088 (2019). DOI: <https://doi.org/10.1007/13369-018-03711-8>
- [9] S.P. Chiew, M.S. Zhao, C.K. Lee, Mechanical properties of heat-treated high strength steel under fire/post-fire conditions. *J. Constr. Steel Res.* **98**, 12-19 (2014). DOI: <https://doi.org/10.1016/j.jcsr.2014.02.003>
- [10] J.C. Villalobos, S.A. Serna, B. Campillo, et al., Evaluation of mechanical properties of an experimental microalloyed steel subjected to tempering heat treatment and its effect on hydrogen embrittlement. *Int. J. Hydrogen Ener.* **42** (1), 689-698 (2017). DOI: <https://doi.org/10.1016/j.ijhydene.2016.10.103>
- [11] J. Liu, L. Wang, Y. Liu, et al., Effects of H content on the tensile properties and fracture behavior of SA508-III steel. *Int. J. Min. Mater.* **22**, 820-828 (2015). DOI: <https://doi.org/10.1007/s12613-015-1139-2>
- [12] M.Q. Wang, E. Akiyama, K. Tsuzaki, Fracture criterion for hydrogen embrittlement of high strength steel. *Mater. Sci. Tech.-Lond.* **22** (2), 167-172 (2006). DOI: <https://doi.org/10.1179/174328406X86191>
- [13] G.P. Tiwari, A. Bose, J.K. Chakravarty, et al., A study of internal hydrogen embrittlement of steels. *Mater. Sci. Eng. A.* **286** (2), 269-281(2000). DOI: [https://doi.org/10.1016/S0921-5093\(00\)00793-0](https://doi.org/10.1016/S0921-5093(00)00793-0)
- [14] M B. Djukic, V. S. Zeravcic, G. Bakic, et al., Hydrogen embrittlement of low carbon structural steel. *Procedia Mater. Sci.* **3**, 1167-1172(2014). DOI: <https://doi.org/10.1016/j.mspro.2014.06.190>
- [15] G. Wang, Y. Yan, J. Li, et al., Hydrogen embrittlement assessment of ultra-high strength steel 30CrMnSiNi2. *Corros. Sci.* **77**, 273-280 (2013). DOI: <https://doi.org/10.1016/j.corsci.2013.08.013>
- [16] Q.S. Allen, T.W. Nelson, Microstructural evaluation of hydrogen embrittlement and successive recovery in advanced high strength steel. *J. Mater. Process Tech.* **265**, 12-19 (2019). DOI: <https://doi.org/10.1016/j.jmatprotec.2018.09.039>
- [17] J. Venezuela, F.Y. Lim, L. Liu, et al., Hydrogen embrittlement of an automotive 1700 MPa martensitic advanced high-strength steel. *Corros. Sci.* **171**, 108726 (2020). DOI: <https://doi.org/10.1016/j.corsci.2020.108726>

- [18] S.K. Saha, B. Moon, C. Lee, et al., Enhancing the hydrogen embrittlement resistance of medium-carbon high-strength steel by optimizing the tempering temperature. *Mater. Charact.* **207**, 113530 (2024). DOI: <https://doi.org/10.1016/j.matchar.2023.113530>
- [19] W. Wang, Y. Zhang, L. Xu, et al., Mechanical properties of high-strength Q960 steel at elevated temperature. *Fire Safety J.* **114**, 103010 (2020). DOI: <https://doi.org/10.1016/j.firesaf.2020.103010>
- [20] GB/T 39281-2020 Wire electrodes, wires, rods and deposits for gas shielded arc welding of high strength steels (In Chinese).
- [21] W.J. Dan, C.W. Tang, H. Shi, et al., Study on Mechanical Behaviours and Microstructure Features of Q690 Steel Weldments with Various Electrochemical Hydrogen Charging Conditions. *Materials* **17** (22), 5446 (2024). DOI: <https://doi.org/10.3390/ma17225446>
- [22] H.T. Lin, Study on microstructure properties and hydrogen embrittlement sensitivity of welded joints of high-strength steel QP980. University of Science and Technology Beijing, China (2020) (In Chinese). DOI: <https://doi.org/10.26945/d.cnki.gb-jku.2020.000238>.
- [23] GB/T 228-1987 Tensile Test Methods for Metals (In Chinese).
- [24] S.A. Afolalu, E.Y. Salawu, O.O. Joseph, et al., Overview Impacts of Heat Treatment Techniques on Grain Structures of a Steel. *Mat. Sci. Eng. B-ADV*, **1107** (1), 012137 (2021). DOI: <https://doi.org/10.1088/1757-899X/1107/1/012137>
- [25] G. Singh, A review on effect of heat treatment on the properties of mild steel. *Mater. Today Commun.* **37**, 2266-2268 (2021). DOI: <https://doi.org/10.1016/j.matpr.2020.07.702>
- [26] R.A. Grange, The rapid heat treatment of steel. *Metall. Trans.* **2**, 65-78 (1971). DOI: <https://doi.org/10.1007/BF02662639>
- [27] K.Z. Zhang, Research on high temperature brittleness mechanism and inhibition method of laser welded joint of Ti2AlNb-based alloy. Harbin Institute of Technology, China (2017) (In Chinese).
- [28] L.I. Kejian, C.A.I. Zhipeng, L.I. Yifei, et al., Influence of long-term aging at elevated temperature on welds with carbon migration. *J. Tsinghua University (Science and Technology)*, **55** (10), 1051-1055 (2015). DOI: <https://doi.org/10.16511/j.cnki.qhdxxb.2015.22.021>
- [29] L. Zhao, S. Wei, D. Wu, et al.,  $\delta$ -ferrite transformation mechanism and its effect on mechanical properties of 316H weld metal. *J. Mater. Sci. Technol.* **57**, 33-42 (2020). DOI: <https://doi.org/10.1016/j.jmst.2020.02.085>
- [30] M.B. Djukic, V.S. Zeravcic, G. Bakic, et al., Hydrogen embrittlement of low carbon structural steel. *Procedia Mater. Sci.* **3**, 1167-1172 (2014). DOI: <https://doi.org/10.1016/j.mspro.2014.06.190>
- [31] S.V. Panin, P.O. Maruschak, I.V. Vlasov, et al., Effect of operating degradation in arctic conditions on physical and mechanical properties of 09Mn2Si pipeline steel. *Procedia Engineering* **178**, 597-603 (2017). DOI: <https://doi.org/10.1016/j.proeng.2017.01.117>
- [32] R.P.M. Procter, Hydrogen degradation of ferrous alloys. *Brit. Corros. J.* **21** (2), 79-80 (1986). DOI: <https://doi.org/10.1179/000705986798272325>
- [33] A. Barnoush, H. Vehoff, Recent developments in the study of hydrogen embrittlement: Hydrogen effect on dislocation nucleation. *Acta Mater.* **58** (16), 5274-5285 (2010). DOI: <https://doi.org/10.1016/j.actamat.2010.05.057>
- [34] D.C. Ahn, P. Sofronis, R.H. Jr. Dodds, On hydrogen-induced plastic flow localization during void growth and coalescence. *Int. J. Hydrogen Ener.* **32** (16), 3734-3742 (2007). DOI: <https://doi.org/10.1016/j.ijhydene.2006.08.047>
- [35] R.A. Siddiqui, H.A. Abdullah, Hydrogen embrittlement in 0.31% carbon steel used for petrochemical applications. *J. Mater. Process Tech.* **170** (1-2), 430-435 (2005). DOI: <https://doi.org/10.1016/j.jmatprotec.2005.05.024>
- [36] X. Zhu, K. Zhang, W. Li, et al., Effect of retained austenite stability and morphology on the hydrogen embrittlement susceptibility in quenching and partitioning treated steels. *Mat. Sci. Eng. A-Struct.* **658**, 400-408 (2016). DOI: <https://doi.org/10.1016/j.msea.2016.02.026>
- [37] O. Barrera, D. Bombac, Y. Chen, et al., Understanding and mitigating hydrogen embrittlement of steels: a review of experimental, modelling and design progress from atomistic to continuum. *J. Mater. Sci.* **53** (9), 6251-6290 (2018). DOI: <https://doi.org/10.1007/s10853-017-1978-5>
- [38] Z. Wang, J. Xu, J. Li, Effect of heat treatment processes on hydrogen embrittlement in hot-rolled medium Mn steels. *Int. J. Hydrogen Energ.* **45** (38), 20004-20020 (2020). DOI: <https://doi.org/10.1016/j.ijhydene.2020.04.241>
- [39] Y. Wang, X. Wu, W. Wu, Effect of  $\alpha'$  martensite content induced by tensile plastic prestrain on hydrogen transport and hydrogen embrittlement of 304L austenitic stainless steel. *Metals-Basel*, **8** (9), 660 (2018). DOI: <https://doi.org/10.3390/met8090660>
- [40] NASA 8-30744 National Aeronautics and Space Administration.
- [41] P.V. Yasniy, I.B. Okipnyi, P.O. Maruschak, et al., Toughness and failure of heat resistant steel before and after hydrogenation. *Theor. Appl. Fract. Mec.* **56** (2), 63-67 (2011). DOI: <https://doi.org/10.1016/j.tafmec.2011.10.001>